

# Modification of the flow structures in a swirling jet

Karlis ATVARIS<sup>1</sup>, Mark THOMPSON<sup>1,2</sup>, Kerry HOURIGAN<sup>1,2</sup>

<sup>1</sup>*Fluids Laboratory for Aeronautical and Industrial Research (FLAIR),*

*Department of Mechanical Engineering, Monash University 3800, Melbourne, Australia*

<sup>2</sup>*Division of Biological Engineering, Monash University 3800, Melbourne, Australia*

*Correspondence: Kerry.Hourigan@eng.monash.edu.au*

**Abstract.** The effect of a downstream bluff body on upstream vortex breakdown has been investigated in an open-flow, motivated by the potential for tissue culture in swirling flow bioreactors. A sphere was placed on the central axis of a swirling jet issuing into a tank of stagnant water. The position of the stagnation point of a vortex breakdown was tracked as a result of varying the azimuthal Reynolds number. While it is known that an increase in azimuthal Reynolds number leads to the upstream movement of the vortex breakdown stagnation point, this investigation focuses on the position of the vortex breakdown as a function of sphere size, axial Reynolds numbers, and sphere position. It was found that the distance from the jet exit to the stagnation point scaled with axial Reynolds number to the half-power, and that distinctive flow topologies of closed and open recirculation zones were found that were analogous to the cone and bubble forms previously found. Varying the size of the sphere was found to affect the flow only for sphere diameters comparable or larger than that of the nozzle — a smaller sphere size was found not to modify the flow significantly from the no-sphere case. Finally, the distance of the sphere from the nozzle affected the stagnation point location in the near-nozzle region. A correlation was also found between the swirl setting for various sphere distances at which the vortex breakdown changed form, with the swirl setting that gave the same stagnation point position with the no-sphere case.

**Key words:** vortex breakdown, bioreactors, stagnation point, bluff-bodies, incompressible flow.

## 1. Introduction

Tissue engineering typically involves cells being seeded through convection on scaffolds in a bioreactor in order to establish a 3D culture. There is a requirement for the tissue cells to be cultured under well-controlled operating conditions and in an optimum environment. The process of tissue culture depends crucially on the supply of soluble nutrients and oxygen. Furthermore, in the case whereby the engineered tissues would need to possess biomechanical properties that are critical to their function *in vivo* (relevant to musculoskeletal tissue engineering), the application of mechanical forces acts as an important modulator of cell physiology.

Different forms of bioreactors for which we have investigated the flow fields include the closed type with a spinning lid plus either a fixed lid [10] or a free surface [4, 5], or an open type with a swirling jet injection below a free surface and an outflow at the bottom [7]. In all these situations and for a range of conditions, a recirculation region, or vortex breakdown bubble, has been observed to occur along the centreline axis. Whether the presence of vortex breakdown in a bioreactor is beneficial or detrimental to tissue engineering is unclear, but certainly optimization of tissue growth requires the control of vortex breakdown.

Many control methods have been tried in an attempt to influence the position and occurrence of vortex breakdown. As described in the review by Mitchell & Delery [9], vortex breakdown generally can be categorised as either pneumatically or mechanically based. In seeking to understand the underlying physics of the open flow vortex breakdown, Billant et al. [2] performed an experiment on a swirling jet issuing into an open tank. This minimised the effects of confinement that could, in addition to the effect of changing flow conditions, influence vortex breakdown onset significantly [11]. Using a rotating honeycomb section in an axial flow, Billant et al. [2] were able to independently vary the rotational and axial velocity of the vortex core. They found, in addition to the known bubble state of vortex breakdown, a cone state, which has no closed recirculation zone. Furthermore, they confirmed the existence of a critical swirl number that determines the onset of vortex breakdown, with the swirl number defined as a ratio of maximum azimuthal and axial components of velocity upstream of breakdown. Interestingly, vortex breakdown was also found to be relatively independent of the axial Reynolds number. Investigations on pneumatic control of vortex breakdown in an open tank are limited: Khalil et al. [7] used a sinusoidal variation in the axial flow rate to alter the shedding frequency of shear-layer vortices, and Gallaire et al. [6] directed radial jets to act on the perimeter of the swirling jet to excite particular mode shapes in the wake of a swirling jet. However, unlike Khalil et al. [7], Gallaire et al. [6] were unable to affect the position or occurrence of breakdown with their shear-layer manipulation. It was suggested that this was because the mechanisms leading to breakdown act on the central region of the jet [12].

In primarily looking at blockage effects in pipe flows, Mattner et al. [8] studied a mechanical method of vortex interaction, by placing a sphere on the central axis of a swirling pipe flow. It was found that for particular swirl settings, a steady recirculation zone could be formed upstream of the sphere surface, which was enclosed by the vortex breakdown shear-layer reattaching to the sphere surface. It was noted that the swirl required to form this upstream stagnation point was significantly less than that required to form breakdown without a sphere. This was not unexpected in light of the work of [3], who theorised that the onset of breakdown was caused by the appearance of negative upstream azimuthal vorticity, the existence of which was confirmed in [8] by interpolating LDV measurements of the flow.

The current investigation aims to extend research into mechanical means of interacting with a vortex core by placing a sphere in an open tank swirling jet. It is intended that some insight can be inferred from these experiments into the behaviour and possibly the mechanism of open-flow vortex breakdown, as well as the modification of bioreactor flows by the presence of tissue culture scaffolds.

## 2. Experimental setup

In this investigation, experiments were performed in an open-tank flow apparatus, as shown in the schematic diagram of Fig. 1 and which is similar to that designed and used by Billant et al. [2]. A large perspex tank of rectangular cross section ( $570 \times 600 \times 1540\text{mm}$ ) is filled with filtered tap-water. A head unit issues a swirling jet of water through an exit nozzle of diameter  $\hat{D}_N = 39.5\text{mm}$ , held well beneath the water level in the tank. The axial component of the jet is generated using a viscous-disk pump, and monitored for consistency via a feedback mechanism from a

## MODIFICATION OF A SWIRLING JET

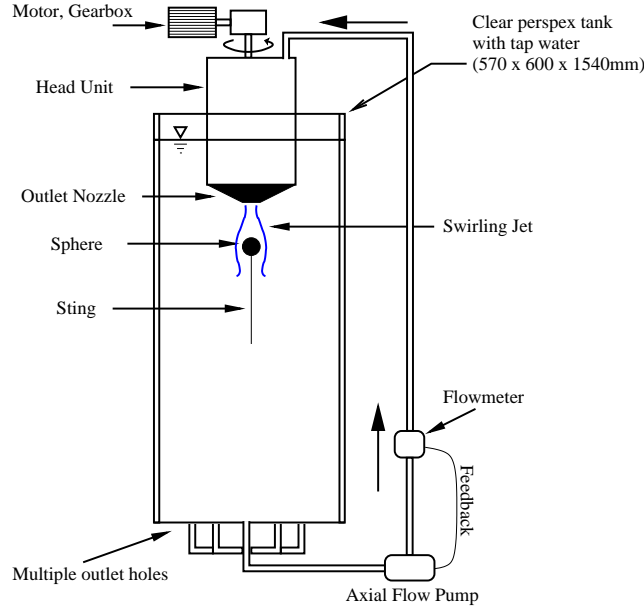


*Figure 1.* Schematic diagram of experimental apparatus. A sphere is placed under the contraction nozzle with a sting attached to the side of the tank. Both motor and pump are controlled separately by computer to generate axial and azimuthal velocity components. Tank, sphere and head unit dimensions are to scale.

magnetic flow meter. The rotational or swirling component of the jet is generated by the rotation of a honeycomb section inside the head unit, and a contraction nozzle is then used to reduce to the size of the jet. Both the axial-flow pump and the motor rotating the honeycomb are controlled by individual motors and motor controllers, allowing independent variation of the axial and rotational velocity components.

Previous studies by Khalil et al. [7] on this particular apparatus have confirmed the axial and azimuthal velocity profiles are comparable with those of Billant et al. [2]. Buoyancy effects can be non-negligible for the flow velocities involved here, as noted by [2], so an attempt was made to reduce thermal effects by allowing the entire rig to equalise in temperature over a period of days by running both motors at speed before experiments commenced. During experiments, the temperature was constantly monitored to ensure flow (and thermal) conditions remained constant.

A short distance downstream of the nozzle outlet, the swirling jet impinges on a sphere of diameter  $\hat{D}_S$ , placed on the central axis of the nozzle at a distance away from the nozzle tip of  $\hat{x}_S$ . Various sphere sizes were used, and each was held in place on the central axis using a  $0.127\hat{D}_N$  diameter sting of a length greater than  $7\hat{D}_N$  and held against the side wall of the tank with a perpendicular arm downstream of the sphere. This allowed the sphere to be held rigidly in position, with no observable movement or vibration when the swirling jet was switched on. Accurate placement under the nozzle was achieved by imaging the sphere-nozzle arrangement from perpendicular positions. The sphere position was measured to be horizontally within 1% of the central axis, and vertically within the measurement uncertainties (typically 3%) of the required distance from the nozzle.

Visualisation was achieved by the use of long exposure photography with a small quantity of particles in the water, giving streak-line images to depict the flow struc-

tures. The flow was illuminated simultaneously from both sides of the tank by a 3mm thick light-sheet made with two apertured 1200W stage-lamps. This method of visualisation ensured only a relatively small number of particles was needed to visualise the flow over the course of experimenting. This had the advantage of not interfering with steady-state flow conditions by having to regularly inject flow-visualisation liquids into the system, or needing to keep filtering the fluid between experiments, such as is required with PLIF. Images were taken using a single 1.3MB CCD Pixelfly camera set perpendicular to both the light sheets and the flow axis, and focused with a 28mm Nikon lens to image only the region around the upstream side of the sphere and the outlet part of the contraction nozzle.

Throughout this investigation, the characteristic length used for scaling was chosen to be the nozzle diameter, because only a single nozzle diameter was used and it is a representative length of the jet. The axial Reynolds number is used as the fundamental flow descriptor of the jet, and defined here in the downstream, or axial direction  $x$ , in terms of dimensional parameters of the volumetric axial flow rate  $Q$ , and the nozzle exit diameter  $\hat{D}_N$ :

$$Re_x = \frac{4Q}{\pi \hat{D}_N \nu}, \quad (1)$$

where  $\nu$  is the kinematic viscosity of the fluid. The amount of swirl imparted on the jet is defined in terms of the rotation speed of the honeycomb section inside the head unit,  $\omega_M$ , and takes the form of a rotational Reynolds number  $Re_\omega$ :

$$Re_\omega = \frac{2\pi\omega_M \hat{D}_N^2}{\nu}. \quad (2)$$

A measure of the system response was given by the stagnation point location  $P = \hat{x}/\hat{D}_N$ , and a key output from this investigation would be a quantitative relationship between this observable and the control variables.

## 2.1. STAGNATION POINT MOVEMENT WITH AXIAL REYNOLDS NUMBER

A sphere of size  $D_S = 1.47 \pm 0.02$  was placed at a distance of  $x_S = 1.99 \pm 0.03$  downstream of the nozzle exit, where  $D_S$  and  $x_S$  are non-dimensionalised by nozzle diameter. Four axial Reynolds numbers were chosen, increasing in steps of 150 from  $Re_x = 450$  to  $Re_x = 900$ , with an uncertainty of  $\pm 20$ . At each swirl setting, the position of the stagnation point was determined. It was found that by plotting the position against a modified non-dimensional swirl parameter, defined as a ratio of the azimuthal Reynolds number to the axial Reynolds number taken to the half power, that the data collapse to a single curve, as shown in Fig. 2(a). A smoothed least-squares spline has also been fitted to the data, to show the trend of the general collapse, and to separate this general collapse from any hysteresis in the stagnation point position, which was evident for the  $Re_x = 600$  and  $Re_x = 750$  cases. The quality of the collapse suggests that the assumption of a power-law scaling for the stagnation point position seems appropriate, and we can conclude that the stagnation point location is a function of  $Re_x^{1/2}$  to good accuracy. It is not yet clear what

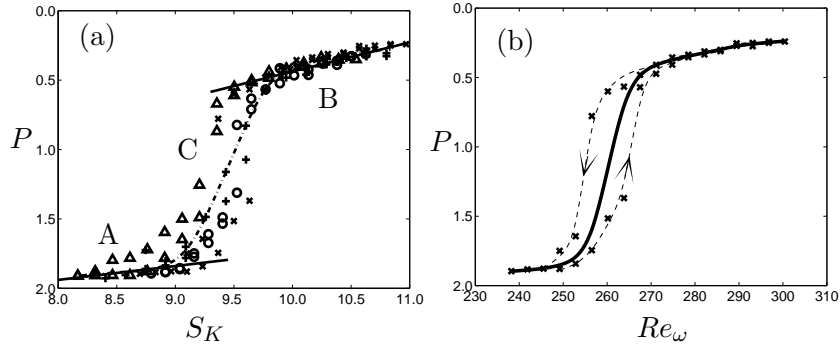


Figure 2. (a) Stagnation point location  $P$  plotted against a rescaled swirl parameter of  $S_K$ , defined as  $S_K = Re_\omega / Re_x^{0.5}$ . Axial Reynolds numbers plotted are (+)  $Re_x = 450$ , ( $\Delta$ )  $Re_x = 600$ , ( $\times$ )  $Re_x = 750$  and ( $\circ$ )  $Re_x = 900$ . (b) Stagnation point location for  $Re_x = 750$  plotted against rotational Reynolds number, demonstrating the apparent hysteresis in stagnation point location by the deviation away from an averaged spline curve. Arrows indicate direction of increasing and decreasing swirl.

the physical significance of this scaling is; however, it is noted that the boundary layer thickness also scales with  $Re_x^{1/2}$ .

The data for  $Re_x = 750$  have been replotted separately in Fig. 2(b) to show the hysteretic behaviour of the stagnation point location as the swirl is increased or decreased. In the figure, increasing swirl corresponds to the points below the average line, and decreasing swirl to those above the line. One reason for this hysteresis in stagnation point position may be found by looking at the flow topologies in the hysteretic region, which are shown in Fig. 3. For increasing swirl, the recirculation zone is upstream of the sphere surface, and the shear-layer reattaches to the sphere surface. But when decreasing the swirl, the stagnation point is closer to the nozzle, and the shear-layer is clear of the sphere. It would appear from this observation that the reason for the observed hysteresis effect in the stagnation point position is that both forms of the vortex breakdown in the near-nozzle and the near-sphere regions are stable states for the same swirl ratio.

A further point is that Billant et al. [2] found hysteresis in the swirl number required for the appearance and disappearance of the vortex breakdown for a similar range of axial Reynolds number,  $Re_x = 626 - 839$ . Although in the present study the hysteresis of breakdown *appearance* was not accurately determined, the *trace* of the stagnation point that displayed hysteresis-like behavior occurred in the same  $Re_x$  range as for Billant et al. [2].

In order to further understand the physics of this flow, we can look at the curve displayed in Fig. 2(a) as consisting of three parts corresponding to distinct flow behaviours. The first, indicated with the letter A, corresponds to when the breakdown is close to the sphere. Here, on increasing the swirl, an upstream stagnation point first occurs, followed by the formation of an upstream recirculation zone between the stagnation point and the sphere surface (as depicted in Fig. 3). This is identical to the flow topology found by Mattner et al. [8], and because the recirculation zone is closed to the outside stagnant flow, it can be said that the vortex breakdown is in a closed form, analogous to the bubble state of breakdown seen by Billant et al. [2]. Increasing rescaled swirl up to  $S_K = 9.0$ , the stagnation point moves steadily

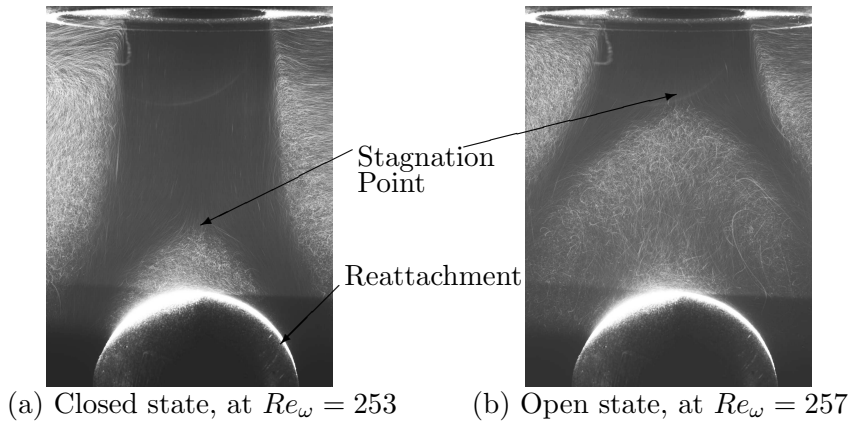


*Figure 3.* Comparison between (a) a closed recirculation zone between the sphere surface and the stagnation point, with the vortex breakdown shear-layer re-attaching to the sphere surface, and (b) an open form of breakdown, with shear-layer clear of sphere surface. Images are taken for  $Re_x = 750$ , and  $D_S = 1.47 \pm 0.02$ ,  $x_S = 1.99 \pm 0.03$ .

upstream in a relatively linear fashion, with the re-attachment point moving downstream of the sphere.

The second region of interest corresponds to when the stagnation point is close to the nozzle exit and well upstream of the sphere, indicated in Fig. 2(a) by the letter B. As mentioned earlier, the vortex breakdown in this higher swirl condition is of an open form, with the shear-layer completely detached from the sphere surface and open to the surrounding flow. The open topology of the flow (depicted in Fig. 3(b)) seems to be very much analogous to the cone-form of breakdown seen by Billant et al. [2], and indeed, a time sequence of this flow shows that the stationary recirculating zones of the closed form of breakdown are here replaced with traveling vortices advecting along and shedding from the shear layer. With the rescaled swirl increasing from  $S_K = 9.5$  to  $S_K = 10.5$ , the stagnation point moves upstream, in much the same manner as with the near-sphere region.

The region C, between regions A and B, corresponds to flow states between these two extremes. At around  $S_K = 9.2$ , flow visualisation shows that the shear-layer region enclosing the recirculation zone has a width comparable to that of the sphere. Small increases in  $Re_\omega$  in this region result in large movements of the stagnation point upstream. It is in this transition region where a unique topology could not be determined because of hysteresis. Of note, Billant et al. [2] found that for a given swirl, the bubble form of breakdown first appeared at a higher swirl ratio than the cone breakdown.

## 2.2. THE EFFECT OF SPHERE SIZE ON STAGNATION POINT LOCATION

For this set of experiments, the axial Reynolds number was kept constant at  $Re_x = 600 \pm 20$ , and two sphere sizes were tested along with a third no-sphere case. The spheres were placed at approximately the same axial distance downstream of the nozzle exit. The smaller sphere diameter was measured to be  $D_S = 0.62 \pm 0.05$  and placed at  $x_S = 0.99 \pm 0.03$ . The larger sphere diameter was measured to be  $D_S = 0.99 \pm 0.02$  and placed at a measured distance of  $x_S = 1.00 \pm 0.02$ .

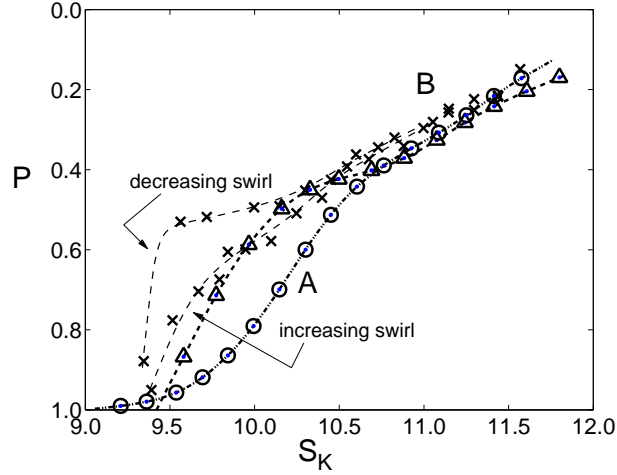


Figure 4. Stagnation point variation with rescaled swirl parameter  $S_K$  for sphere sizes of  $D_S = 0.62(\triangle)$  and  $D_S = 0.99(\circ)$  placed at one nozzle diameter downstream. The no-sphere case data has been plotted ( $\times$ ) along with the a least-squares spline fit of the data.

The tracking of the stagnation point with swirl has been plotted in Fig. 4, and can be seen to comprise two distinctive regions. The first, marked by the letter A, is where the onset of the upstream stagnation point occurs. For the case of the smaller sphere, the stagnation point moves rapidly upstream as swirl is increased to  $S_K = 10.0$ , where it reaches a position (scaled on the nozzle diameter)  $P = 0.5$  away from the nozzle. Increasing the swirl further beyond this position moves the stagnation point upstream in a fairly steady and linear fashion. These general trends are shown also with the no-sphere case, which we note is hysteretic, but a linear fit of the near-nozzle region gives a gradient of  $-0.23D_N/S_K$ . The close matching of these two cases can be seen by the flow topologies, which are shown in Fig. 5(a) and (b). It can be seen that the shear-layer for the small-sphere case is clear of the sphere surface, and has the same shape as for the no-sphere case. Even when the stagnation point is close to the small-sphere surface, the shear-layer simply continues undisturbed past the sphere into the general flow, maintaining the same cone-angle as the stagnation point moves upstream.

The flow visualisation for the larger sphere case in Fig. 5(c) shows that for sufficient sphere size, the flow structure can be modified. Here, the stagnation point movement in the low-swirl section is significantly different to the previous two cases, in that the breakdown is in a closed form. From the data of Fig. 4, as swirl is increased for the larger-sphere case, the upstream recirculation region grows in size and the stagnation point moves upstream, keeping the shear layer attached to the sphere surface. This is much the same type of motion observed in the previous section (Sec. 2.1) Only once the stagnation point reaches a height of around  $P = 0.5$  does the shear layer detach from the sphere, and the stagnation point moves upstream at the same rate as the small-sphere and no-sphere cases.

These separate paths of stagnation point movement for different sphere sizes suggest that there exists a critical sphere size, of between  $D_S = 0.62$  and  $D_S = 0.99$ , that determines whether the breakdown in the near-sphere region will be an open or closed form, and so whether the stagnation point will move upstream at a fast or

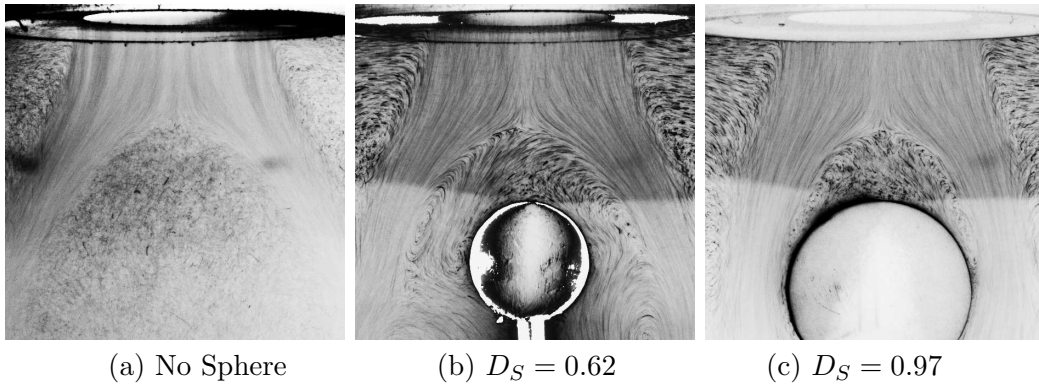


Figure 5. Flow visualisation of the same stagnation point location for the cases of (a) no-sphere at  $S_K = 9.6$ , (b)  $D_S = 0.62$  at  $S_K = 9.7$  and (c)  $D_S = 0.99$  at  $S_K = 10.3$ . The shear-layer of the vortex breakdown region for the larger sphere is attached to the sphere surface but open for the smaller sphere, as for the no-sphere case. Images taken at  $Re_x = 600$ .

slow rate with increasing swirl.

Significantly, however, is the near-nozzle region indicated in Fig. 4 by the letter B and deals with the steady upstream movement of the stagnation point in the upper-swirl range starting from around  $S_K = 10.4$ . Here, the plot shows the same linear movement of the stagnation point towards the nozzle with increasing swirl as seen in Sec. 2.1. Also, the breakdown in this region is in an open form, with the shear-layer clear of any contact with the sphere surface.

### 2.3. SPHERE POSITION EFFECT ON STAGNATION POINT LOCATION.

The single sphere of size  $D_S = 0.99 \pm 0.02$  was placed at distances of  $x_S = 0.75, 1.00, 1.50, 2.00$  and  $2.50$  away from the nozzle outlet. The axial Reynolds number was once again held constant at  $Re_x = 600 \pm 20$ .

The results of tracking the stagnation point for all five sphere positions are shown in Fig. 6, together with the data of the no-sphere case of Sec. 2.2. Plotted is the distance from the nozzle, measured in nozzle diameters, against the modified swirl parameter  $S_K$ . Once again, the stagnation point data of the measured stagnation point position are represented by a least-square spline of the averaged data.

The first feature of note in Fig. 6 is that towards the higher swirl setting, ( $> S_K = 10.7$ ), the stagnation point location paths for all sphere positions seem to converge in a similar upward trend, much as in the near-nozzle regions of the previous sections.

The second feature of this plot is that the paths traced out for the individual sphere locations eventually cross over that of the no-sphere case. The reasons for this are not entirely clear, but a clue as to its significance can be found from looking at the flow visualisations. For each sphere location case, the swirl setting for which the path of each sphere location curve in Fig. 6 crosses that of the no-sphere case is summarised in Table 1 as  $Re_\omega^*$ . The swirl value at which the shear-layer can be seen to detach from the surface of the sphere is indicated in the same table as  $Re_\omega^\dagger$ , and is in very good agreement with  $Re_\omega^*$ , to well within 10%.

This analysis indicates that, although the presence of the sphere is able to keep the breakdown in a closed form close to the sphere surface, once the stagnation

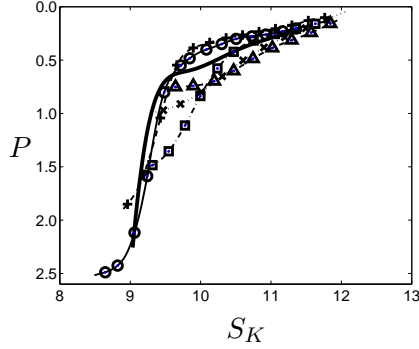


Figure 6. Least-squares spline fits of averaged stagnation point location against the swirl parameter of Sec. 2.2 for various sphere positions:  $(\Delta)x_S = 0.75$ ,  $(\times)x_S = 1.0$ ,  $(\square)x_S = 1.5$ ,  $(+)x_S = 2.0$ ,  $(\circ)x_S = 2.5$ . Dark solid line represents data of the no-sphere case.

$x_S$	$Re_\omega^*$ ( $\pm 4$ )	$Re_\omega^\dagger$
1.0	276	285 ( $\pm 3$ )
1.5	255	256 ( $\pm 2$ )
2.0	236	237 ( $\pm 2$ )
2.5	230	226 ( $\pm 2$ )

Table 1. Comparison of the swirl setting for complete detachment of the shear-layer from the surface of the sphere.  $Re_\omega^*$  is measured from Fig. 6 where the stagnation point location path of each sphere crosses that of the no-sphere case, and  $Re_\omega^\dagger$  is determined from observing flow visualisations.

point reaches a height that it would ordinarily be at in a no-sphere case, the shear-layer detaches from the sphere surface. It can also be seen in the plot of Fig. 6 that there appears to be an overshoot of the stagnation point location above the no-sphere position once the shear-layer has detached. This is a significant finding, since if the criticality theory developed by [1] were to hold, it would be expected that varying the downstream sphere position should not alter the upstream flow conditions. However, it is not immediately obvious why the no-sphere case position gives an indication of when the shear layer detaches from the sphere surface.

### 3. Conclusions

A novel and comprehensive empirical investigation was performed into the effects of a bluff body on the vortex breakdown in a swirling jet in an open flow. While systematically changing flow conditions and bluff body parameters, the stagnation point of the vortex breakdown was monitored as a measure of the system response. It was shown that with increasing rotational Reynolds number ( $Re_\omega$ ), the stagnation point location moved upstream linearly in the near-nozzle and near-sphere regions of the flow topology. By scaling  $Re_\omega$  inversely by axial Reynolds number ( $Re_x$ ) to the power of  $1/2$ , all data collapsed to a single, well-defined curve. It was also shown that, although sphere size appeared not to affect the behaviour of the stagnation point in the near-nozzle region of the flow, there did appear to be a critical sphere size in the range  $0.62 < D_S < 0.99$  that determined whether for a particular  $Re_\omega$

the breakdown upstream of the sphere surface would be in an open or closed state. When the sphere location was varied, it was shown that a good correlation existed between the stagnation point position at which the vortex breakdown shear-layer detached from the sphere surface, and that of the no-sphere case at the same  $Re_\omega$ . Further increasing  $Re_\omega$  beyond this point resulted in a stagnation point location moving closer to the nozzle than for the same  $Re_\omega$  of the no-sphere case.

## Acknowledgments

This research was partly supported under Australian Research Council's Discovery Projects funding scheme (project number DP0452664).

## References

- [1] T.B. Benjamin. Theory of the vortex breakdown. *J. Fluid Mech.*, 14:593–629, 1962.
- [2] P. Billant, J.-M. Chomaz, and P. Huerre. Experimental study of vortex breakdown in swirling jets. *J. Fluid Mech.*, 376:183–219, 1998.
- [3] G. L. Brown and J. M. Lopez. Axisymmetric vortex breakdown. part 2. physical mechanisms. *J. Fluid Mech.*, 221:553–576, 1990.
- [4] J. Dusting, J. Sheridan, and K. Hourigan. A fluid dynamics approach to bioreactor design for cell and tissue culture. *Biotechnology and Bioengineering*, 2006.
- [5] A. Fouras, J. Dusting, and K. Hourigan. A simple in-situ calibration technique for stereoscopic particle image velocimetry. *Experiments in Fluids*, published online March 28, 2007.
- [6] F. Gallaire, S. Rott, and J.-M. Chomaz. Experimental study of a free and forced swirling jet. *Phys. Fluids*, 16(8):2907–2917, 2004.
- [7] S. Khalil, M.C. Thompson, and K. Hourigan. Response of unconfined vortex breakdown to axial pulsing. *Phys. Fluids*, 18(3):38102–1–4, March 2006.
- [8] T.W. Mattner, P.N. Joubert, and M.S. Chong. Vortical flow. part 2. flow past a sphere in a constant-diameter pipe. *J. Fluid Mech.*, 481:1–36, 2003.
- [9] A.M. Mitchell and J. Delery. Research into vortex breakdown control. *Prog. Aerospace Sci.*, 37:385–418, 2001.
- [10] L. Mununga, K. Hourigan, M.C. Thompson, and T. Leweke. Confined flow vortex breakdown control using a small disk. *Physics of Fluids.*, 16(12):4750–4753, 2004.
- [11] T. Sarpkaya. On stationary and travelling vortex breakdown. *J. Fluid Mech.*, 45(3):545–559, 1971.
- [12] S. Wang and Z. Rusak. The dynamics of a swirling flow in a pipe and transition to axisymmetric vortex breakdown. *J. Fluid Mech.*, 340:177–223, 1997.